REPORT DOCUMENTATION PAGE

Form Approved
OMB No. 0704-0188

1. REPORT DATE *(DD-MM-YYYY)*	2. REPORT TYPE	3. DATES COVERED *(From - To)*
05-12-2011	Conference Paper	

4. TITLE AND SUBTITLE

A Finite Element Approach for Multidimensional Inverse Heat Conduction

5a. CONTRACT NUMBER

5b. GRANT NUMBER

5c. PROGRAM ELEMENT NUMBER

6. AUTHOR(S)
E. Coy, M. Bergkoetter, S. Danczyk and E. Felix

5d. PROJECT NUMBER

5f. WORK UNIT NUMBER
50250548

7. PERFORMING ORGANIZATION NAME(S) AND ADDRESS(ES)

Air Force Research Laboratory (AFMC)
AFRL/RZSA
10 E. Saturn Blvd.
Edwards AFB CA 93524-7680

8. PERFORMING ORGANIZATION REPORT NUMBER

9. SPONSORING / MONITORING AGENCY NAME(S) AND ADDRESS(ES)

Air Force Research Laboratory (AFMC)
AFRL/RZS
5 Pollux Drive
Edwards AFB CA 93524-7048

10. SPONSOR/MONITOR'S ACRONYM(S)

11. SPONSOR/MONITOR'S NUMBER(S)
AFRL-RZ-ED-TP-2011-573

12. DISTRIBUTION / AVAILABILITY STATEMENT

Distribution A: Approved for public release; distribution unlimited. PA# 111039.

13. SUPPLEMENTARY NOTES
For presentation at the AIAA 50th Aerospace Sciences Meeting

14. ABSTRACT

An efficient technique for mapping thermal boundary conditions is described and demonstrated. The technique is based on a piece-wise polynomial approximation where the Laplacian derivatives in space are constrained using the heat equation. Measured values for the Laplacian are obtained from temperature rate measurements from sensors embedded within a body. The technique has been implemented in a digital signal processor and is able to provide real-time data on thermal boundary conditions over a surface. The technique is adaptable to complex geometry. In this paper the technique is applied to a study of the injector-wall interactions in a laboratory scale liquid rocket engine.

15. SUBJECT TERMS

16. SECURITY CLASSIFICATION OF:			17. LIMITATION OF ABSTRACT	18. NUMBER OF PAGES	19a. NAME OF RESPONSIBLE PERSON
					Dr. Edward B. Coy
a. REPORT	b. ABSTRACT	c. THIS PAGE	SAR	15	19b. TELEPHONE NUMBER *(include area code)*
Unclassified	**Unclassified**	**Unclassified**			N/A

A Finite Element Approach for Multidimensional Inverse Heat Conduction

Edward B. Coy[1] and Matthew Bergkoetter[2], Stephen A. Danczyk[3], Edgar Felix[4]
Air Force Research Laboratory, Edwards AFB,CA,93524

An efficient technique for mapping thermal boundary conditions is described and demonstrated. The technique is based on a piece-wise polynomial approximation where the Laplacian derivatives in space are constrained using the heat equation. Measured values for the Laplacian are obtained from temperature rate measurements from sensors embedded within a body. The technique has been implemented in a digital signal processor and is able to provide real-time data on thermal boundary conditions over a surface. The technique is adaptable to complex geometry. In this paper the technique is applied to a study of the injector-wall interactions in a laboratory scale liquid rocket engine.

Nomenclature

a_i	=	a constant in a polynomial, also a dimension
d	=	vector of data
$\boldsymbol{G}$	=	a matrix of polynomial terms
$\boldsymbol{P}$	=	a vector of polynomials
q	=	heat flux
T	=	temperature
t	=	time
W	=	plate thickness
x,y,z	=	dimensional coordinates
σ	=	a complex constant
ω	=	angular frequency
$*$	=	complex conjugate
$\sim$	=	frequency domain variable
^{T}	=	transpose
$^{-1}$	=	inverse

I. Introduction

Local concentrations of heat flux and temperature are of interest in aerospace applications including injector-wall interactions in liquid rocket engines, shock-shock interactions in external flow over hypersonic vehicles, internal and external flow over blades and vanes in gas-turbine engines, and deposition of directed energy. Accurate characterization of the distributions may be required for validation of a model, optimization of a design, or control of an operational system. There are two basic methods in use today. In the calorimetry approach a heat exchanger is incorporated into the wall of the device and the temperature rise of the working fluid is used to determine the local heat flux. This method is limited to applications where the heat flux is slowly varying in time and changes in one direction only along the surface. Various assumptions and approximations are required to infer the surface temperature; although, in some cases, temperature sensors can be incorporated to give direct measurements. To obtain high spatial resolution with a calorimeter, specialized manufacturing processes are required. The other major class of methods is appropriate for transient situations which commonly occur in hypersonic wind tunnel test articles and laboratory scale combustion devices where the test articles are designed as heat-sink devices. Surface junction

[1] Mechanical Engineer, Aerophysics Branch, 10 East Saturn Blvd., AIAA Member
[2] Physicist, Aerophysics Branch, 10 East Saturn Blvd.
[3] Research Scientist, Aerophysics Branch, 10 East Saturn Blvd., AIAA Member
[4] Mechanical Engineer, Aerophysics Branch, 10 East Saturn Blvd., AIAA Student Member

thermocouples have been developed which match the thermal characteristics of the test articles and can be treated as non-intrusive to the flow of heat. From the temperature history a heat flux history can be constructed. In some situations the temperature sensors must be embedded in the wall at some distance from the surface. In this situation, inverse methods must be used to reconstruct the surface heat flux and temperature[1]. The mathematical methods for performing the analysis for surface junction and embedded sensors have been extensively studied and are highly developed; however the most widely used methods assume that the flow of heat is one-dimensional. The potential errors in this approach can be readily appreciated when one considers the situation that occurs when heat is deposited by a concentrated source such as a laser. When energy is deposited adjacent to the sensor, heat diffuses in the plane of the surface causing a temperature rise at the location of the sensor which is recorded incorrectly as heat flux at that point. Due to a plethora of such applications, research in this area has shifted to the development of solution techniques for spatially multi-dimensional and transient problems.

The mathematical characteristics of the inverse heat conduction problem are well known. Changes in boundary conditions cause attenuated and time-lagged responses within a body. In the presence of noise and measurement error, the problem becomes ill-posed and solutions can be biased and unstable. Successful inverse techniques have been developed which rely on the use of information from future time steps to ensure that changes in the boundary conditions at the current time step have had time to reach the sensor locations. Stabilization has also been accomplished through Tikhonov regularization. Other techniques utilize low-order basis functions to dampen instabilities. Most techniques rely on an iterative solution wherein an initial estimate for the boundary condition is made, followed by a forward calculation to establish the effect at the sensor locations, and then a refinement in the boundary condition with repetition until a stopping criteria is satisfied. The need to solve the forward problem multiple times at each time step in a transient analysis results in lengthy run times and must be performed in post-processing. In addition to the destabilizing effects of noise and measurement error and the time required to complete a calculation, practical methods must also contend with the temperature dependence of thermal properties, complex geometries, the need to accurately model the effects of temperature sensor installations, have the ability to handle transient and steady state applications, and be intelligible to those responsible for applying the technique.

II. Theory

In the one-dimensional approximation[2], the temperature profile within a body can be approximated with a polynomial.

$$T(z) \approx P_n(z) = c_0 + c_1 z + \ldots + c_n z^n \tag{1}$$

In general, n+1 measurements are required to solve for the n+1 coefficients. Multiple measurements can be obtained from a single sensor if we make use of the heat equation to relate spatial second derivatives with time derivatives. If we consider two sensors that are placed at two depths, and a P_3 approximation, we have the following solutions.

$$T(0) = T(z_1)\frac{z_2}{z_2 - z_1} - T(z_2)\frac{z_1}{z_2 - z_1} + \frac{\partial^2 T(z_1)}{\partial z^2}\frac{z_1 z_2 (2z_2 - z_1)}{6(z_2 - z_1)} + \frac{\partial^2 T(z_2)}{\partial z^2}\frac{z_1 z_2 (z_2 - 2z_1)}{6(z_2 - z_1)} \tag{2}$$

$$q(0) = -k(T_0)\left(T(z_1)\frac{-1}{z_2 - z_1} + T(z_2)\frac{1}{z_2 - z_1} + \frac{\partial^2 T(z_1)}{\partial z^2}\frac{z_1^2 - 2z_1 z_2 - 2z_2^2}{6(z_2 - z_1)} + \frac{\partial^2 T(z_2)}{\partial z^2}\frac{2z_1^2 + 2z_1 z_2 - z_2^2}{6(z_2 - z_1)} \right) \tag{3}$$

Higher order approximations can be constructed using spatial fourth derivatives and/or a larger number of sensors. In the one-dimensional approximation the spatial second derivatives are obtained from the heat equation.

$$\frac{\partial^2 T}{\partial z^2} = \frac{1}{\alpha}\frac{\partial T}{\partial t} \tag{4}$$

A correction for the effects of temperature gradients normal to the z-direction can be made using adjacent sensors to form a finite-difference approximation to the Laplacian derivative.

$$\frac{\partial^2 T}{\partial x^2} = \frac{T(x-l,z) - 2T(x,z) + T(x+l,z)}{l^2} + O(l^2) \tag{5}$$

$$\frac{\partial^2 T}{\partial z^2} \approx \frac{1}{\alpha}\frac{\partial T}{\partial t} - \frac{T(x-l,z) - 2T(x,z) + T(x+l,z)}{l^2} \tag{6}$$

The accuracy of the correction for lateral diffusion can be evaluated by comparing with analytical solutions. A suitable test case is a semi-infinite body exposed to a step change in heat flux over half the surface and insulated over the other half[3]. The dimensional quantities used in the test case were chosen to be representative of a device and test conditions described later in this paper. The edge of the heated region is located at the centerline, x=0. The model contains nine pairs of temperature sensors at depths of z_1=1.65 mm and z_2=5.21 mm, with a lateral spacing of l=4.23 mm. The heat flux used in the simulations was 5 W/mm^2. The material properties of the solid were reference values for copper, k=400 W/m-K and α=117 mm^2/s.

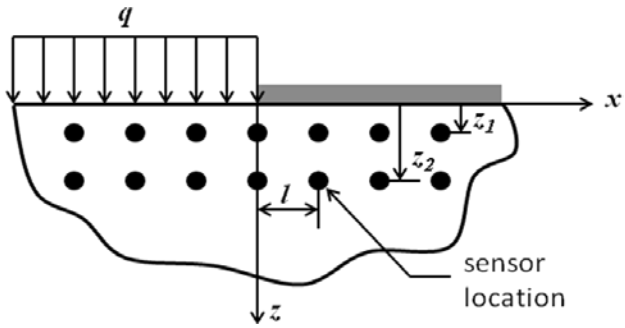

Figure 1 Validation case. Semi-infinite body with uniform heat flux over half the face.

Figure (2) contains heat flux results for the one-dimensional approximation, equation (4), and the corrected 1D approximation, equation (6), which is labeled 2D in the figure. There is a significant improvement achieved by accounting for the lateral diffusion of heat. At the centerline where the edge of the heated region is located, the predicted heat flux is the average value. Figure (3) shows the prediction of surface temperature. The 2D approximation achieves a better agreement with the analytical solution, although surface temperature is a less sensitive quantity to predict.

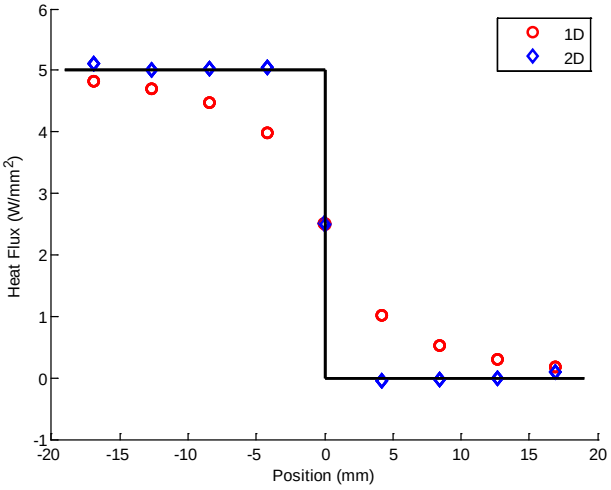

Figure 2 Heat Flux t=1 s

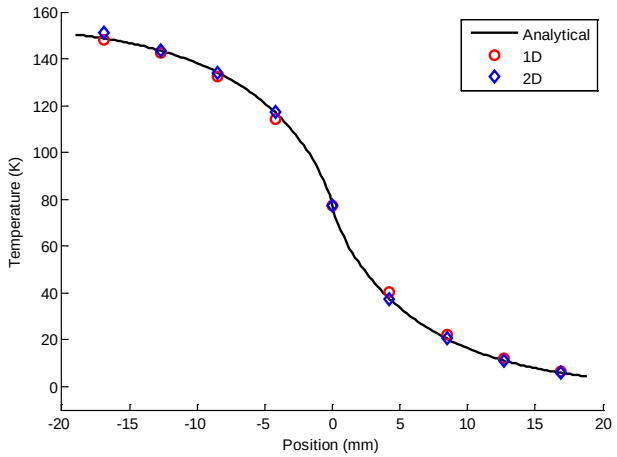

Figure 3 Surface Temperature t=1 s

Figures (4) and (5) show simulated effects of noise in the temperature measurements and the sensor locations. The random error in temperature was assumed to be 1 K and the random error in sensor locations in both x and z directions was assumed to be 0.1 mm. These are representative values based on experience. Twenty simulations were conducted with random errors generated from a uniform distribution. The estimated error in the heat flux for the simulated conditions is in the range of +/- 0.5 W/mm^2 and the estimated error in the surface temperature is +/- 5 K. These values depend on many factors. To get as accurate an estimate as possible the simulated conditions need to mimic the test conditions. In general, the fractional uncertainty decreases with increasing heat flux.

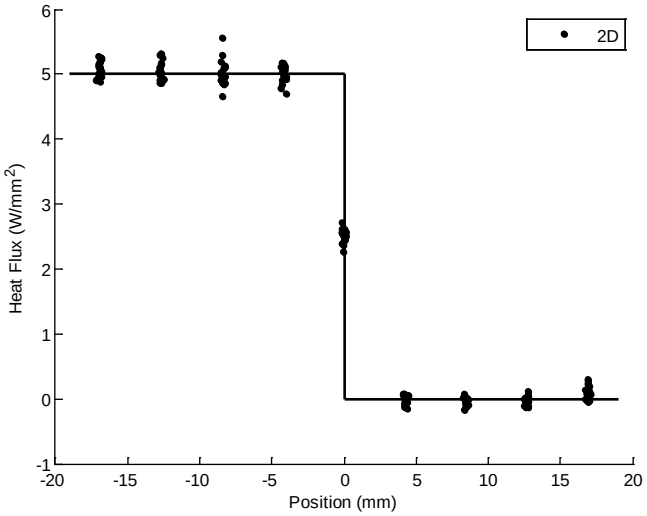

Figure 4 Noised data σ_x=0.1mm, σ_T=1K

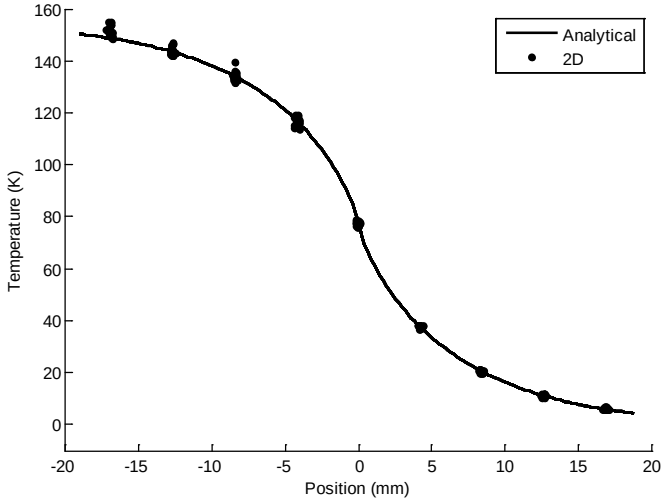

Figure 5 Noised data, σ_x=0.1mm, σ_T=1K

III. Validation

Substitution calibration of heat flux sensors for liquid rocket engine applications is not possible because there is no reference standard available. Estimates of accuracy must rely on analysis of the sources of error. In addition to the factors already discussed in Section II, the sources of error include systematic errors in the temperature measurements, the thermal transport property correlations, and the assumptions used in deriving the mathematical model. In this section we describe tests we used to quantify these sources of error. The method is based on the following analytical solution to the one-dimensional heat equation for a semi-infinite domain with a steady-periodic heat flux at the surface.

$$T(x,t) = T_0 + \frac{\overline{q}}{k}\left(\frac{\alpha}{\omega}\right)^{\frac{1}{2}} \exp\left(-z\left(\frac{\omega}{2\alpha}\right)^{\frac{1}{2}}\right)\cos\left(\omega t - z\left(\frac{\omega}{2\alpha}\right)^{\frac{1}{2}} - \frac{\pi}{4}\right) \tag{7}$$

If we can show our assumptions are valid for the conditions of equation (7), then they must also be valid for equations (2) and (3). The advantage of using equation (7) is that we can avoid the measurement of an absolute level of heat flux and instead base the validation on a measurement of thermal diffusivity which is well known. The measurement is made by exposing a heat flux sensor to a steady periodic heat source and feeding the output of the temperature sensors into a lock-in amplifier capable of measuring phase angle. The thermal diffusivity is obtained from the following expression derived from the phase angle.

$$\alpha = \frac{\omega}{2}\left(\frac{z_2 - z_1}{\theta_2 - \theta_1}\right)^2 \tag{8}$$

If the measured thermal diffusivity does not agree with the reference value, the errors may be due to thermocouple placement, thermocouple time response, multidimensional heat flow, or impurities in the material. Equation (8) will not identify the source of error but it is unlikely that there will be cancelling errors that lead fortuitously to a correct thermal value of thermal diffusivity.

In the following figure we show an example of errors due to multi-dimensional heat flow. A carbon-tube furnace (Thermogauge Instruments Model HT-7000A) was used as a heat source and an optical chopper (New Focus 3501) was used to create a square wave input at 0.5 Hz. The phase angles were measured with a digital lock-in amplifier (Signal Recovery 7265). The sensor element was a cylindrical rod of copper (Alloy 101), 12.5 mm in diameter and

50 mm long, pressed into a copper cylinder, 19.1 mm in diameter and 50 mm long, with two type-K thermocouples pressed into grooves on opposing sides of the inner rod. The sheaths were stripped back exposing the thermocouple wires. An alumina insulator was placed over the wires to avoid contact between the wires and the sheath, between the wires themselves, or between the wires and the base material at an incorrect point. The wires were pressed into circumferential grooves in the inner rod and the junctions were formed through the base material in the intrinsic configuration. As the opening in the chopper wheel swept across the surface of the sensor, it first passed over one thermocouple location and then the other, thereby creating a flow of heat that was not one-dimensional. Rotating the sensor on its axis caused the relative position of the two sensors to shift and resulted in a varying value for the measured thermal diffusivity.

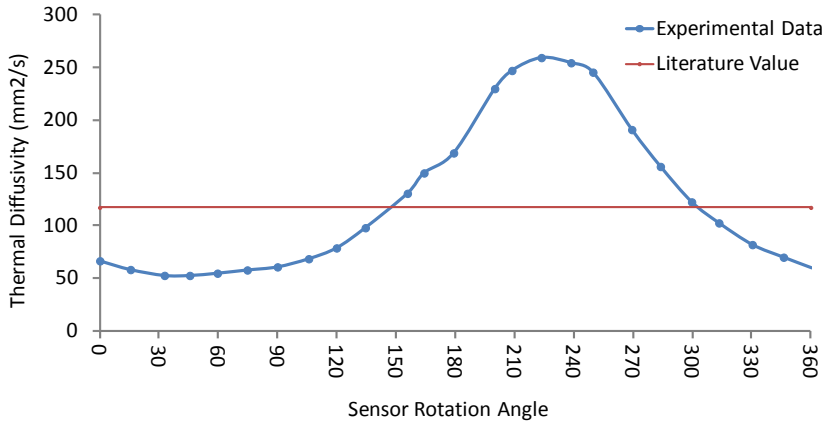

Figure 4 Erroneous thermal diffusivity due to multidimensional heat flow

The experiment was repeated with the optical chopper replaced with a fast shutter (Uniblitz VMM-T1 driver and CS45 shutter). In this case, both thermocouple locations received simultaneous exposure and the thermal diffusivity results were much improved. These results validate the method with respect to the method used to install thermocouples, the thermal property correlations, and the assumptions used in the derivation of the one-dimensional model. The results also illustrate the importance of accounting for multidimensional heat flow. The results of Section II above validate the extension to multidimensional heat flow.

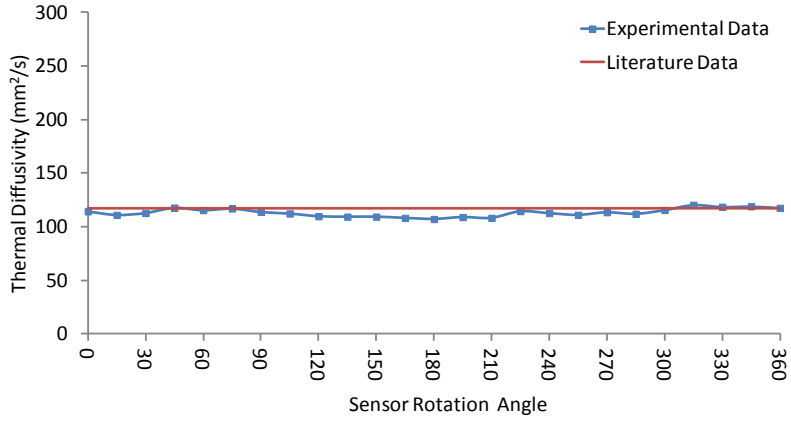

Figure 5 Results with one-dimensional heat flow.

III. Implementation

The code that implements equations (2) and (3) in the test facility runs on a Pacific Instruments model 6042 card, which is built around a Texas Instruments Model TMS320C6711 Floating Point Digital Signal Processor capable of 900 million floating point operations per second at a clock rate of 150MHz. The PI card's firmware includes a finite impulse response filter function as well as basic matrix/array addition and multiplication which are accessible through the PI660 GUI software from Pacific Instruments. For the sake of convenience, the current implementation is built from these basic operations in the PI660 environment, although a lower-level implementation compiled using the TI processor's software development kit (SDK) could be expected to improve efficiency. The current method has been demonstrated with 32 channels at a rate of 1000 Hz. The major steps in the implementation are as follows:

1. Load pre-calculated constants before the system starts taking data
2. Load data from DAQ backplane to DSP memory
3. Calculate temperature values from raw voltage
4. FIR filter data (smoothing and differentiating)
5. Estimate thermal diffusivity α at each sensor location based on linear fitting coefficients for $\alpha(T)$
6. Matrix multiplication for $T(0)$ and quantity in parenthesis in eq. (3)
7. Estimate thermal conductivity k for each of the surface temperature values using a linear fit of $k(T)$
8. Find q on the surface using $k(T(0))$
9. Send results back to DAQ system

IV. Application

The target application for this effort was the characterization of injector-wall interactions in liquid rocket engine combustion chambers. Most chamber failures occur due to localized concentrations of heat flux. High heat flux and high oxygen concentrations impinging on the chamber wall can lead to a phenomena known as blanching[4]. We are interested in creating a capability for screening candidate injector designs for this type of behavior in lab-scale tests to avoid costly redesigns of full-scale engines.

For this study we screened two injector types. The first was a gas-centered swirl co-axial element (GCSC)[5,6] operating with gaseous oxygen and RP-2, a liquid hydrocarbon propellant. The second was an array of 25 shear, co-axial elements operating with gaseous oxygen and gaseous hydrogen. In both cases we characterized the heat flux patterns produced by the injectors in an as-built condition and after "defects" were deliberately created. The gas-centered swirl coaxial element design is shown in Figure (7). The cylindrical passage is referred to as the post and is for the gaseous oxygen. The post includes three liquid injection orifices near the downstream end. The liquid enters the central cylinder tangentially to generate a swirling liquid film around the inner diameter of the post. The liquid film is thus subjected to a combination of cross-flow shear and centrifugal forces. The liquid is stripped from the film inside the element by the central gas jet, which entrains the droplets and transports the resultant spray downstream. In this study we blocked one of the three fuel injection orifices in an attempt to create a non-uniform spray pattern and wall heat flux.

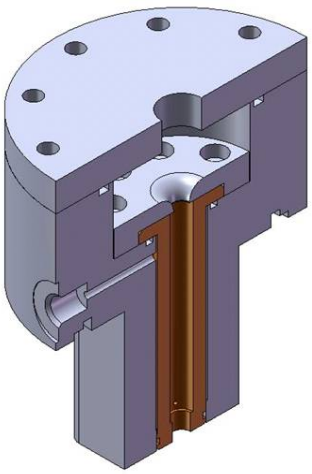

Figure 7 Lab-scale gaseous-oxygen, co-axial swirled injector

The 25 element array of shear co-axial injector elements is shown in Figure (8). The gaseous oxygen enters from the left. It first encounters a distribution plate and then enters the oxygen posts. Each oxygen post contains a precision orifice pressed into the inlet. The hydrogen enters through the openings in the top and bottom and flows through passages in the oxygen-post support plate and then the annular gaps between the oxygen posts and the face plate. To create non-uniformity, the inlet orifice in the oxygen post closest to the wall between the centerline and wall was blocked.

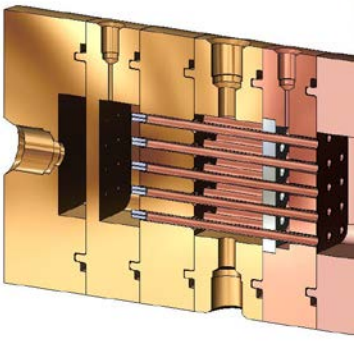

Figure 6 Lab-scale shear co-axial injector elements

The measurement device was located 38 mm from the face plate. It consisted of a block of copper with nine pairs of embedded thermocouples. The pairs were oriented perpendicular to the direction of gas flow to capture streaks. The thermocouple junctions were formed through the copper base material using the technique of intrinsic thermocouples to ensure a fast time response. An alumina insulator was used to ensure that the only point of contact for the thermocouple wires was on the copper surface at the bottom of the hole. The thermocouple wires were terminated on an Iso-Tech TRU 100 Multi-Channel TC Referencing Unit and data were recorded on Pacific Instruments Model 6013 cards in a PI 660 DAQ system at 1000 Hz with 16 bit resolution and conditioned with 25 Hz 4-pole Bessel filters.

The heat flux and temperature distributions for the two injectors in the as-built and defect configurations are shown in Figures (7)-(10). The data shown was taken immediately prior to the end of the run. The heat flux profile for GCSC is highly uniform for the as-built configuration and skewed for the defect configuration. The co-ax is skewed for both configurations. Surface temperatures follow the same trends but are skewed for all cases due to residual effects of the torch igniter that created an initially skewed temperature profiles as it fired across the face of the injector during startup. There are no significant streaking patterns observed under any conditions. In future work we will compare these measurements with predictions using a CFD code.

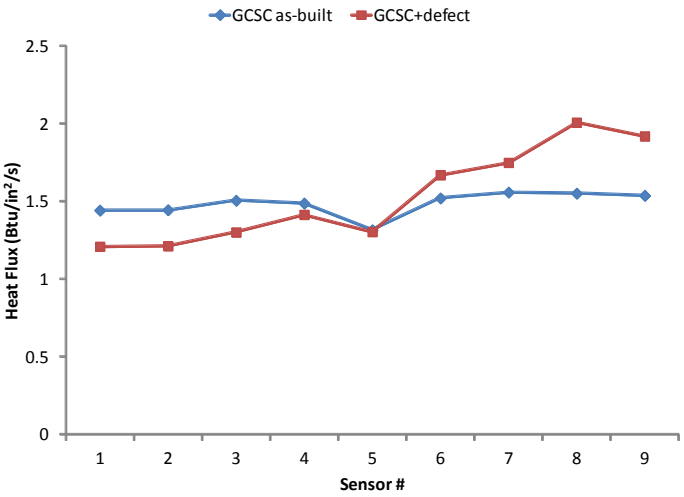

Figure 7 Heat flux distributions for GCSC injector

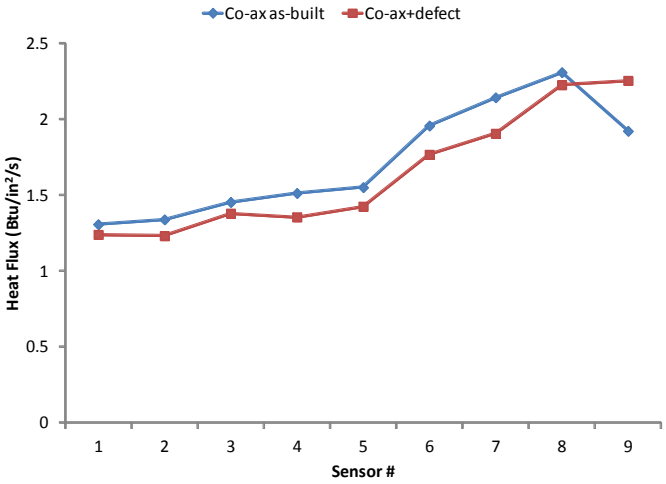

Figure 8 Heat flux distributions for shear co-ax injectors

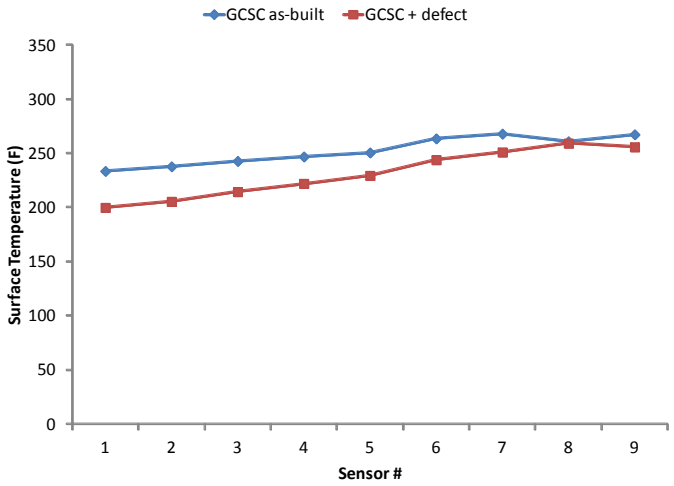

Figure 9 Surface temperature distributions for GCSC injector

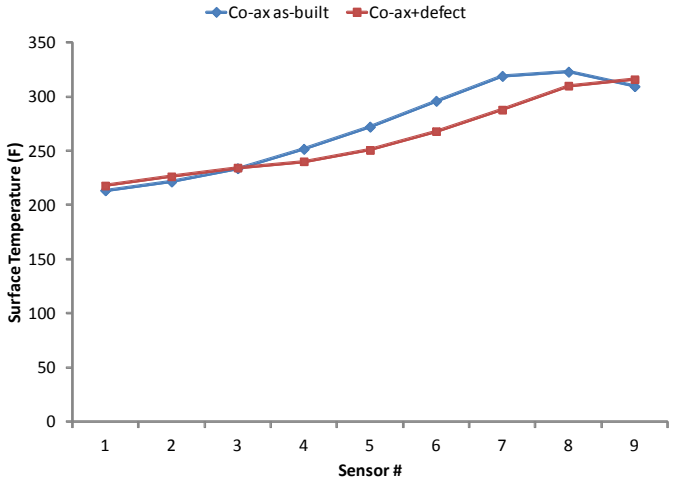

Figure 10 Surface temperature distributions for shear co-ax injectors

V. Multidimensional Approach

In this final section we provide some preliminary results on an extension of the general method described in Section II to higher dimensions. We utilize the strategy of domain decomposition. Finite element methods are highly developed for forward problems. They are used because the basic approach of subdividing the domain into cells and approximating the solution over each cell with a polynomial is readily adaptable to complex geometries and is mathematically tractable. However, there are some distinct differences between forward and inverse problems that result in some changes in the basic strategy. In solving forward problems it is possible to generate meshes that are limited in size only by the memory capacity of the computer. It is possible to finely discretize regions where the function behavior is complex such that, within each individual cell, the function can be approximated adequately with a simple linear basis function. In inverse problems, as developed here, the grid corresponds to a network of sensors. In practical applications, grids with tens or hundreds of nodes are possible, but probably not thousands, and certainly not the millions that are now common in forward problems. This provides a strong impetus for developing schemes that use high order basis functions. Coy showed how basis functions of arbitrary order can be developed in one spatial dimension using two nodes by constraining the approximating polynomials using the even numbered

spatial derivatives from the heat equation. Adding second derivatives improved the frequency response by three orders of magnitude. The model could be formulated as a digital filter and calculated in real time. In this paper we extend the approach to three dimensions.

To fix ideas we consider a set of sensors embedded in a solid material with smoothly varying thermal transport properties. We are primarily interested in constructing approximations for the temperature and heat flux distribution at the surface. The temperature distribution at any point in time within each finite element is approximated by a polynomial.

$$T(x,y,z,t) \approx a_0 + a_1 x + a_2 y + a_3 z + a_4 xy + a_5 xz + a_6 yz + \cdots \tag{1}$$

Or simply as,

$$T(\boldsymbol{x},t) \approx \boldsymbol{P}^{\boldsymbol{T}}\boldsymbol{a} \tag{2}$$

Where,

$$\boldsymbol{P}^{\boldsymbol{T}} = [1 \;\; x \;\; y \;\; z \;\; xy \;\; xz \;\; yz \;\; \ldots] \tag{3}$$

$$\boldsymbol{a} = [a_0 \;\; a_1 \;\; a_2 \;\; a_3 \;\; a_4 \;\; a_5 \;\; a_6 \;\; \ldots]^T \tag{4}$$

A grid of sensors may enable a finite-difference estimate of the Laplacian in the plane of the surface. In this case, the second derivative normal to the surface can be estimated as,

$$\frac{\partial^2 T}{\partial z^2} = \frac{1}{\alpha}\frac{\partial T}{\partial t} - \nabla^2_{xy} T$$

The time derivatives can be obtained from the temperature records at the measurement points. The set of equations to be solved can be written,

$$\begin{bmatrix} \boldsymbol{P}^{\boldsymbol{T}}(\boldsymbol{x_1}) \\ \vdots \\ \boldsymbol{P}^{\boldsymbol{T}}(\boldsymbol{x_n}) \\ \dfrac{\partial^2 \boldsymbol{P}^{\boldsymbol{T}}(\boldsymbol{x_1})}{\partial z^2} \\ \vdots \\ \dfrac{\partial^2 \boldsymbol{P}^{\boldsymbol{T}}(\boldsymbol{x_n})}{\partial z^2} \end{bmatrix} \begin{bmatrix} a_1 \\ \vdots \\ a_m \end{bmatrix} = \begin{bmatrix} T_1 \\ \vdots \\ T_n \\ \dot{T}_1/\alpha_1 \\ \vdots \\ \dot{T}_n/\alpha_n \end{bmatrix} \tag{7}$$

Or simply as,

$$\boldsymbol{G}\boldsymbol{a} = \boldsymbol{d} \tag{8}$$

If the number of equations exceeds the number of terms in the polynomial, we can solve as a least-squares problem.

$$\boldsymbol{a} = (\boldsymbol{G}^{\boldsymbol{T}}\boldsymbol{G})^{-1}\boldsymbol{G}^{\boldsymbol{T}}\boldsymbol{d} \tag{9}$$

Note that $(\boldsymbol{G}^{\boldsymbol{T}}\boldsymbol{G})^{-1}\boldsymbol{G}^{\boldsymbol{T}}$ depends only on the location of the sensors.

The performance of the method can be evaluated by comparing with analytical solutions. Cole has developed Green's function solutions for steady-periodic heating that are suitable for this purpose. Consider a uniform slab of depth W and infinite width with a uniform, single-frequency, steady-periodic heat flux on the surface at y=W, -a<x<a.

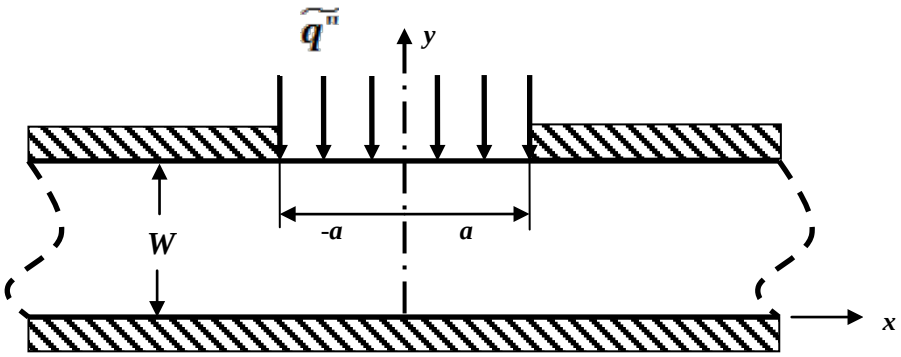

The temperature inside the slab can be expressed as,

$$T(x,y,t) = Real\left[\tilde{T}(x,y,\omega)\, e^{j\omega t}\right] \tag{10}$$

$$\tilde{T}(x,y,\omega) = \frac{\alpha q_0}{k}\left[\frac{1}{W}\int_{-a}^{a}\frac{e^{-\sigma_0|x-x'|}}{2a\sigma_0}dx' + \sum_{n=1}^{\infty}(-1)^n\frac{2}{W}cos\left(\frac{n\pi}{W}y\right)\int_{-a}^{a}\frac{e^{-\sigma_n|x-x'|}}{2a\sigma_n}dx'\right]$$

$$\sigma_n = \left[\left(\frac{n\pi}{W}\right)^2 + j\omega/\alpha\right]^{1/2}$$

$$\int_{-a}^{a}\frac{e^{-\sigma_n|x-x'|}}{2a\sigma_n}dx' = \begin{cases} \dfrac{e^{\sigma_n x}\sinh(a\sigma_n)}{a\sigma_n^2}, & x < -a \\ \dfrac{2 - e^{-\sigma_n(a+x)} - e^{-\sigma_n(a-x)}}{2a\sigma_n^2}, & -a < x < a \\ \dfrac{e^{-\sigma_n x}\sinh(a\sigma_n)}{a\sigma_n^2}, & x > a \end{cases}$$

We will use the analytical function to obtain inputs to the finite element model, and again to compare the amplitude and phase of the analytical function with predictions of the finite element model at points distant from the sensor locations, most importantly at the surface. The model coefficients are real constants that multiply the data vector so we can write,

$$\tilde{\boldsymbol{a}} = (\boldsymbol{G}^T\boldsymbol{G})^{-1}\boldsymbol{G}^T\tilde{\boldsymbol{d}} \tag{11}$$

$$\tilde{\boldsymbol{d}} = \begin{bmatrix} \tilde{T}_1 \\ \vdots \\ \tilde{T}_n \\ j\omega\tilde{T}_1/\alpha_1 \\ \vdots \\ j\omega\tilde{T}_n/\alpha_n \end{bmatrix} \tag{12}$$

The complex temperature predicted by the finite element model can be written,

$$\tilde{T}(\boldsymbol{x}) = \boldsymbol{P}^T\tilde{\boldsymbol{a}} \tag{13}$$

The complex heat flux in the z-direction is,

$$\tilde{q}_{FE}(x) \approx -k\frac{\partial P^T}{\partial z}\tilde{a} \tag{14}$$

The gain and phase-lag of the finite element model relative to the analytical solutions are the following,

$$\Gamma(x,\omega) = \frac{[\tilde{T}_{FE}\cdot\tilde{T}^*_{FE}]^{1/2}}{[\tilde{T}\cdot\tilde{T}^*]^{1/2}} \tag{15}$$

$$\varphi(x,\omega) = atan[Imag(\tilde{T}_{FE})/Real(\tilde{T}_{FE})] - atan[Imag(\tilde{T})/Real(\tilde{T})] \tag{16}$$

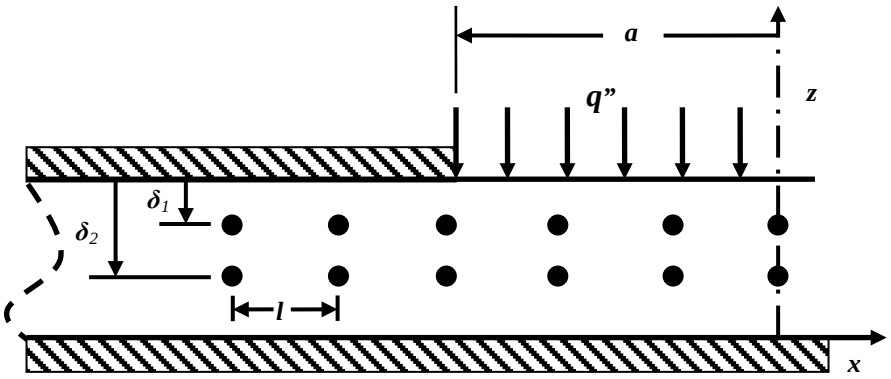

At locations $x = \pm a$ there are gradients of temperature in the x-direction that we would like to capture. We take as a length scale the distance from the heated surface to the first sensor, δ_1. Thus we have, $\delta_1^+ = 1, \delta_2^+ = \delta_2/\delta_1, a^+ = a/\delta_1, l^+ = l/\delta_1, W^+ = W/\delta_1, x^+ = x/\delta_1, z^+ = z/\delta_1$. Temperature and frequency are non-dimensionalized as follows: $\tilde{T}^+ = \tilde{T}k/q_0 a$, and $\omega^+ = \omega\delta_1^2/\alpha$. We consider a case where a^+ and W^+ are large and look at the effect of frequency, ω^+, on the surface temperature, $\tilde{T}^+$, amplitude and phase for several values of the sensor spacing, l^+.

Figure 11 illustrates the methods ability to reconstruct a complex surface temperature distribution. The figure shown is taken from a transient simulation that illustrates the methods ability to reproduce full images of the thermal boundary conditions in real time.

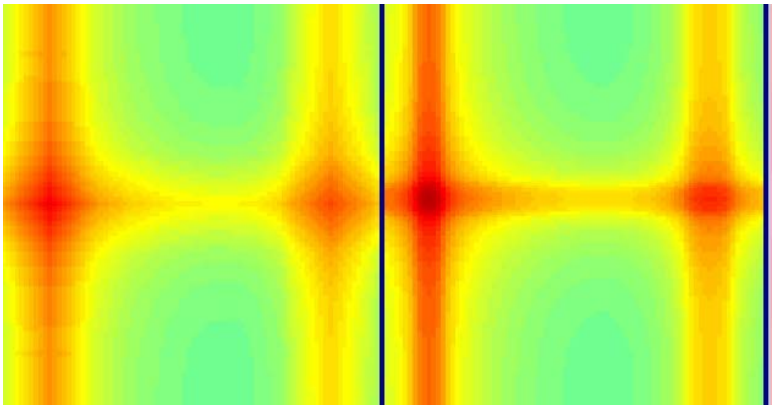

Figure 11 Full panel simulation with three band heat sources and piecewise polynomial reconstruction. The left panel is an 8x8 cell reconstruction and the right cell is the analytical solution.

VI. Conclusion

Direct measurement of complex, transient, thermal boundary conditions is often not possible in aerospace applications and inverse techniques using embedded sensors must be used. Existing techniques for resolving the inverse problem are computationally intensive and cannot be performed in real time or even on a post-processing time scale that supports test schedules. In this paper we describe a technique that addresses all of these technical challenges and illustrate its application in the characterization of injector-wall interactions in a lab-scale liquid rocket engine combustion chamber. Data was acquired from two injector types in an as-built configuration and with defects introduced in an initial attempt to assess the sensitivity of the designs to manufacturing flaws. In addition to the analytical model, we include an experimental characterization of the method's accuracy and a description of its implementation using a digital signal processor. A further generalization and extension of the technique to multi-dimensional, transient problems for arbitrary geometries is described.

---

[1] Beck, J.V., Blackwell, B., St. Clair, C.R., "Inverse Heat Conduction," Wiley-Interscience, 1985

[2] Coy, E.B., "Measurement of Transient Heat Flux and Surface Temperature Using Embedded Temperature Sensors," Journal of Thermophysics and Heat Transfer, Vol. 24, No. 1, pp. 77-84, 2010

[3] Cole, K.D., Beck, J.V., Haji-Sheikh, A., Litkouhi, B., "Heat Conduction Using Green's Functions, 2nd ed.," CRC Press, Taylor and Francis Group, 2011

[4] Tucker, P., Rybak, J., Hulka, J., Jones, G., Nesman, T.,, West, J., "The NASA Constellation Universities Project: Thrust Chamber Assembly Virtual Institute,' AIAA-2006-4524, 42nd AIAA/ASME/SAE/ASEE Joint Propulsion Conference, Sacremento, CA, 2009

[5] Strakey, P.A., Cohn, R.K., Talley, D.G., "The Development of a Methodology to Scale Between Cold-Flow and Hot-Fire Evaluations of Gas-Centered Swirl Coaxial Injectors," ILASS Americas, 17th Annual Conference on Liquid Atomisation and Spray Systems, Arlington, VA, 2004

[6] Schumaker, S., Danczyk, S., Lightfoot, M., "Effect of Cup Length on Film Profiles in Gas-Centered Swirl-Coaxial Injectors," AIAA-2010-368, 48th AIAA Aerospace Sciences Meeting, Orlando, FL, 2010